Effects of substrate temperature, substrate orientation, and energetic atomic collisions on the structure of GaN films grown by reactive sputtering

Ziani S. Schiaber, Douglas M. G. Leite, José R. R. Bortoleto, Paulo N. Lisboa-Filho, and José H. D. da Silva

---

Articles you may be interested in

The properties and deposition process of GaN films grown by reactive sputtering at low temperatures
J. Appl. Phys. **99**, 073503 (2006); 10.1063/1.2186380

Growth stresses and cracking in GaN films on (111) Si grown by metal-organic chemical-vapor deposition. I. AlN buffer layers
J. Appl. Phys. **98**, 023514 (2005); 10.1063/1.1978991

Properties of radio-frequency-sputter-deposited GaN films in a nitrogen/hydrogen mixed gas
J. Appl. Phys. **97**, 093516 (2005); 10.1063/1.1888027

Effect of growth temperature on morphology, structure and luminescence of Eu-doped GaN thin films
Appl. Phys. Lett. **85**, 4890 (2004); 10.1063/1.1825619

Growth condition dependence of structure and surface morphology of GaN films on (111)GaAs substrates prepared by reactive sputtering
J. Vac. Sci. Technol. A **22**, 1290 (2004); 10.1116/1.1765133

CrossMark
click for updates

Effects of substrate temperature, substrate orientation, and energetic atomic collisions on the structure of GaN films grown by reactive sputtering

Ziani S. Schiaber,[1] Douglas M. G. Leite,[2] José R. R. Bortoleto,[3] Paulo N. Lisboa-Filho,[1] and José H. D. da Silva[1,a)]

[1]*Universidade Estadual Paulista, UNESP, Bauru, São Paulo 17033-360, Brazil*
[2]*Universidade Federal de Itajubá, UNIFEI, Itajubá, Minas Gerais 37500-903, Brazil*
[3]*Universidade Estadual Paulista, UNESP, Sorocaba, São Paulo 18087-180, Brazil*

The combined effects of substrate temperature, substrate orientation, and energetic particle impingement on the structure of GaN films grown by reactive radio-frequency magnetron sputtering are investigated. Monte-Carlo based simulations are employed to analyze the energies of the species generated in the plasma and colliding with the growing surface. Polycrystalline films grown at temperatures ranging from 500 to 1000 °C clearly showed a dependence of orientation texture and surface morphology on substrate orientation (*c*- and *a*-plane sapphire) in which the (0001) GaN planes were parallel to the substrate surface. A large increase in interplanar spacing associated with the increase in both *a*- and *c*-parameters of the hexagonal lattice and a redshift of the optical bandgap were observed at substrate temperatures higher than 600 °C. The results showed that the tensile stresses produced during the film's growth in high-temperature deposition ranges were much larger than the expected compressive stresses caused by the difference in the thermal expansion coefficients of the film and substrate in the cool-down process after the film growth. The best films were deposited at 500 °C, 30 W and 600 °C, 45 W, which corresponds to conditions where the out diffusion from the film is low. Under these conditions the benefits of the temperature increase because of the decrease in defect density are greater than the problems caused by the strongly strained lattice that occurr at higher temperatures. The results are useful to the analysis of the growth conditions of GaN films by reactive sputtering. © *2013 AIP Publishing LLC.*
[http://dx.doi.org/10.1063/1.4828873]

I. INTRODUCTION

GaN films are currently being used in a large number of optical and electronic devices, and several other potential applications are being developed.[1–6] In particular, the increasing use of light emitting diodes (LEDs) in a variety of lightning devices represents large-scale energy savings and considerable benefits to the environment.[5,7–9] The main deposition techniques by which the highest quality films are produced with the highest control are molecular beam epitaxy (MBE)[10–12] and metalorganic chemical vapor deposition (MOCVD).[13–16] However, because these techniques are complex and expensive, the search for simpler and more versatile techniques capable of producing high quality homogeneous GaN films over large areas has attracted interest.[7,17–27]

Among the techniques under development for GaN growth based on physical processes are pulsed laser deposition (PLD)[28] and sputtering.[17–26,29–31] In the case of reactive sputtering, significant improvement has been achieved,[17–27,31] including the growth of epitaxial single crystal GaN, which was obtained by using magnetron-sputtering epitaxy (MSE).[23,24,27]

Film growth involving sputtering has some important characteristics. Concerning the versatility of the technique, the use of a pure metallic Ga source in association with N_2 and Ar plasma generation is a simpler alternative to the use of metalorganics or Knudsen cells used in the MOCVD and MBE

techniques. In particular, the sputtering deposition may lead more naturally to large areas as well as rapid and continuous growth, with several advantages concerning large-scale production. Regarding the growth process, the energetic bombardment of the growing film surface by energetic atoms with energies considerably above the common thermal distributions produces significant changes in the structure and morphology of the film.[32–35] If on one side, the energetic collisions can produce different kinds of defects in the material; on the other, the energy provided by the plasma opens up the possibility of depositing high quality films at lower temperatures. The detailed understanding of the complex kinetics of the growth in association with the production of defects in order to produce high quality material is a main challenge to the development of this technique.[17–27,29,30,36]

Molecular dynamics simulations[37,38] showed that much less damage by the undesired effects of ion bombardment is produced in GaN than in Si, Ge, or GaAs during the film growth.[37,38] This remarkable difference (about a factor of 5) is explained by the higher threshold displacement energy of atoms in GaN and favors tests on the sputtering deposition of GaN in relation to other common functional semiconductors. Nevertheless, the complex growth kinetics involving energetic interactions well above the thermal distributions is challenging. Few studies have investigated the combined influence of the energetic particle bombardment during the growth of GaN in association with substrate temperature and orientation.[39–41] Powel *et al.*[41] reported results for N_2^+ impingement using

a)electronic mail: jhdsilva@fc.unesp.br

reactive ion MBE with energies in the 35–90 eV range. However, no previous study has provided a detailed analysis of the combined effects of substrate orientation and temperature, and the impingement of energetic plasma particles on GaN films deposited using RF in reactive sputtering films.

The purpose of the present investigation is to analyze the combined effects of the impingement of energetic particles from the plasma and the effects of diffusion generated by the substrate temperature during the growth of GaN films by reactive magnetron sputtering. The relationships between the deposition parameters and the structure of the films are focused upon in the analysis.

II. EXPERIMENTAL AND SIMULATION DETAILS

The films were grown using a conventional RF magnetron sputtering setup with a pure Ga (99.99999%) source and a mixture of Ar (99.9999%) and N_2 (99.9999%) gases. The system was upgraded with an UHV Design EPI-100 substrate holder with graphite resistance heating and molybdenum substrate holder to allow depositions as high as $1000\,^\circ$C. The target-to-substrate distance was 50 mm. The total working pressure (1.5×10^{-2} torr), the nitrogen gas flow (10 sccm), and deposition time (180 min) were kept constant in all depositions. The Ar flow rates, substrate temperature, and other relevant parameters are presented in Table I.

The low melting point of Ga ($29\,^\circ$C) produces the melting of the target during chamber baking and substrate heating

stages, and sputtering process. The stainless steel chamber, sealed with conflat flanges, was equipped with a commercial sputtering gun, pumping, mass flow, pressure control, and gas analyzer. An Edwards Vacuum EPM 100 balanced magnetron sputtering gun (100 mm target diameter) adapted with a machined stainless steel cup to hold the liquid Ga was used. A small glove box ($0.30 \times 0.30 \times 0.30$ m) was adapted to the entrance of the deposition chamber using a throttle valve. Hence, highly pure Ga was introduced to the target in N_2 pressure under very low contact with moisture, dust, and other contaminants. The residual pressure was better than and 5×10^{-8} torr before starting the heating of the substrate, and 1×10^{-6} torr just before gas admission. The residual gas analysis showed that the main contaminants were H_2 ($\sim 3 \times 10^{-7}$ torr), H_2O (2×10^{-7} torr), and CO($\sim 2 \times 10^{-7}$ torr). The substrates were heated at $800\,^\circ$C for 2 hours just before the depositions. This was expected to produce the thermal cleaning of the sapphire without producing undesirable effects.[42] Concerning the target, two characteristics of the depositions contributed to minimize poisoning of its surface. The first was the use of Ar/N_2 (1:1 and 2:1) mixtures instead of pure N_2; the second was the liquid characteristic of the target, which occurred from the very beginning of the depositions because of pre-heating the substrates. In addition, the target was sputtered for 20 min in pure Ar and then in a mixture of $Ar+N_2$ for 5 min prior to the depositions in order to clean the target surface and to establish nearly regular nitrogen contamination of the target surface before depositions.

TABLE I. Deposition conditions and basic sample parameters. Target: Ga metallic; diameter: 100 mm; distance to substrate: 50 mm. Total pressure: 1.5×10^{-2} torr. Deposition time: 180 min. Nitrogen gas flow rate: 10 sccm.

Substrate Temperature (°C)	RF Power (W)	Vbias (V)	Ar Flow (sccm)	Thickness (nm)	Bandgap (eV) (+/−0.05)	Sample label	Substrate
500	30	282	20	745	3.47	SP136_B	silica
500	30	282	20	781	3.48	SP136_C′	sapph. c-plane
500	30	282	20	720	3.49	SP136_D′	sapph. a-plane
800	30	278	20	458	3.19	SP137_B	silica
800	30	278	20	482	3.22	SP137_C	sapph. c-plane
800	30	278	20	430	3.17	SP137_D	sapph. a-plane
100	45	353	10	832	3.32	SP147_B	silica
100	45	353	10	825	3.32	SP147_C	sapph. c-plane
100	45	353	10	720	3.32	SP147_D	sapph. a-plane
300	45	351	10	1041	3.31	SP144_B	silica
300	45	351	10	980	3.29	SP144_C	sapph. c-plane
300	45	351	10	961	3.28	SP144_D	sapph. a-plane
500	45	348	10	996	3.30	SP146_B	silica
500	45	348	10	936	3.32	SP146_C	sapph. c-plane
500	45	348	10	887	3.32	SP146_D	sapph. a-plane
600	45	343	10	840	3.36	SP142_B	silica
600	45	343	10	831	3.29	SP142_C	sapph. c-plane
600	45	343	10	801	3.27	SP142_D	sapph. a-plane
700	45	346	10	660	3,30	SP145_B	silica
700	45	346	10	636	3.28	SP145_C	sapph. c-plane
700	45	346	10	548	3.25	SP145_D	sapph. a-plane
800	45	341	10	646	3.29	SP148_B	silica
800	45	341	10	592	3.26	SP148_C	sapph. c-plane
800	45	341	10	541	3.26	SP148_D	sapph. a-plane
1000	45	338	10	304	3.27	SP150_B	silica
1000	45	338	10	285	3.22	SP150_C	sapph. c-plane
1000	45	338	10	282	3.31	SP150_D	sapph. a-plane

The RF power (13.6 MHz) was kept constant at either 30 W or 45 W during the depositions of the studied series of samples. The mean values of the V_{bias} during the depositions presented small, approximately linear decrease from 353 to 338 V with the increase in the substrate temperature. The obtained films were very stable and uniform on all substrates and in the deposition conditions used. The only exception was the deposition at 1000 °C. In this condition, the surfaces of films and substrates were covered by a powder of very small particles when removed from the deposition chamber. This powder was easily removable from the surface.

The X-ray diffraction (XRD) experiments were performed using a Rigaku Ultima 2000^{+} setup with a Cu anode and Ni filter. The grazing incidences XRD (GIXRD) were measured at a fixed incidence angle of 1.5°. The ω-scans were measured using 2θ fixed at the values of the peak maxima found by the GIXRD scans. The rocking curves were limited to $\omega \sim 2\theta_{Bragg}$ of each peak because of the single axis configuration of the setup. The reciprocal space mapping was made using Phillips model Xpert PRO MPD triple axis diffractometer, with Cu electrode and diffracted beam monochromator.

Optical transmittance spectra at normal incidence in the 200–3300 nm range were obtained on a Perkin-Elmer Lambda 1050 double-beam spectrophotometer. The refractive index, absorption coefficient, and film thickness were obtained from the transmittance data by using a computational routine based on the Cisneros method.[43] The method uses the complete solutions of Maxwell equations for homogeneous absorbing films onto transparent thick substrates by which the coherent multiple reflections in the film and incoherent multiple reflections in the substrate are taken into account. The maxima and minima of transmittance in the transparent and weakly absorbing regions at energies below the bandgap were used in the routine to determine the refractive index dispersion and film thickness. The set of refined refractive index values corresponding to the energies of the transmittance maxima and minima were used in the single-oscillator model developed by Wemple and DiDomênico[44] to calculate the dispersion of the refractive index. The values of thickness derived from this procedure showed excellent agreement with the scanning electron microscopy (SEM) images of the cross sections of the films.

The absorption coefficients were determined using the exponential dependence of the transmittance on the absorption coefficient, and an iterative procedure for solving the corresponding equations. The rapidly converging calculations assured very precise determination of the absorption coefficient as a function of the photon energy in the absorption edge.[43]

Atomic force microscopy (AFM) and SEMs were used to characterize the sample morphology. The AFM measurements were taken using a Park Systems, model XE-100 in the non-contact mode with Si tips (nominal diameters of 10 nm). The SEM images were taken using a FEI Magellan 400 L microscope operated at 1 kV in secondary electron mode.

The simulations were performed using the transport of ions in matter (TRIM) code developed by Ziegler and Biersack.[45,46] Two calculation steps were used. In the first

step, the deposition parameters, like the V_{bias} potential and deposition pressure, were used as input to calculate the interactions of the ions with the target. The full cascades TRIM procedure was used in this step. In the second step, the resulting energetic particles emerging from the target were used as input in the analysis of the transit of particles from the target to the substrate through the gas. In this step, the less detailed and quicker Kinchin-Pease[47] procedure was adopted. The results of the simulations are displayed in Tables II and III.

III. RESULTS

The deposition parameters, thicknesses, and bandgaps of the films are shown in Table I. The optical constants were obtained from calculations of the absorption edge and nearby low absorption (interference) regions. The film thickness is plotted against substrate temperature for different substrates in Fig. 1. The vertical dashed lines represent the limits of the Movchan–Demchishin–Thornton[32,33,48] zone scheme, where the depositions with temperatures lower than 30% of the melting[49] correspond to the first (Z_1) and energy enhanced (Z_T) zones, while higher temperatures ($T_s > 500$ °C) correspond to the second zone (Z_2). An initial slight increase in thickness (up to $T_s = 300$ °C) and a subsequent continuous decrease (500 °C $\leq T_s \leq$ 1000 °C) were observed. The latter corresponded approximately to the Z_2 region. A slight tendency of the glass substrates to produce greater thicknesses and of the *a*-plane sapphire to produce smaller thicknesses was observed.

Calculations of the energy of the species arriving at the substrate were performed in two steps. In the first step, the collisions of Ar$^+$ and N$^+$ ions with the Ga target with energies equivalent to the bias potential ($\sim$350 eV) resulted in sputtered Ga and backscattered Ar and N (Table II). The mean values of the kinetic energy of species leaving the target were 22, 21, and 94 eV, respectively. When the species leave the target, they must cross the plasma region before reaching the substrate. The parameters corresponding to this crossing are introduced in the second step. Because of the relatively low energy density in the plasma, this crossing

TABLE II. TRIM[45,46] estimation of yields, ranges, and kinetic energies of ion collisions with a Ga target.

Fixed input parameters/conditions:
Ga target, 100 A thick
Type of damage calculation: Full cascades.
Impingements normal to the surface
Number of events: 5000

Incident N$^+$ ion, 350 eV
Range: 22 A, straggle 13 A
Sputtering yield = 0.98 atoms/ion (Ga/N)
Backscattered N: $\langle K \rangle_N = 94 \pm 59$ eV
Ga sputtered by N: $\langle K \rangle_{Ga(N)} = 18 \pm 25$ eV

Incident Ar$^+$ ion, 350 eV
Range: 13 A, straggle 8 A
Sputtering yield = 1.49 atoms/ion (Ga/Ar)
Backscattered Ar: $\langle K \rangle_{Ar} = 21 \pm 19$ eV
Ga sputtered by Ar: $\langle K \rangle_{Ga(Ar)} = 22 \pm 39$ eV

GaN - Reactive Sputtering
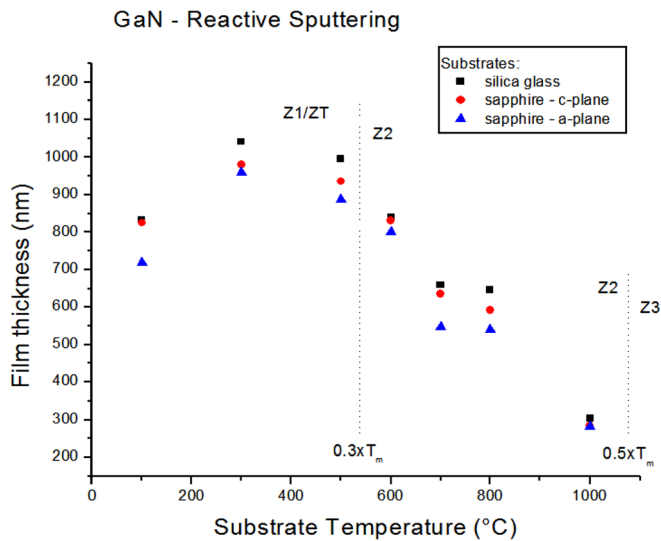
FIG. 1. Thickness of GaN films deposited using constant deposition times as a function of the substrate temperature. The deposition power was kept at 45 W. Different symbols refer to different substrates: black squares = amorphous silica, red circles = c-plane sapphire, blue triangles = a-plane sapphire. The vertical dotted lines represent the limits of the temperature zones, referred to the melting temperature of GaN ($T_m = 2700$ K).

TABLE III. Monte-Carlo TRIM[45,46] calculations of average energy of the species after crossing the Ar+N$_2$ gas, and colliding with the growing film surface.

Fixed input parameters/conditions:
Ar + N$_2$ gas
room temperature
density = 2.72×10^{-8} g/cm^3
layer thickness = 50 mm
Type of damage calculation: Kinchen-Pease (quick)
Impingement normal to the gas layer
Number of events: 5000

Expected (mean) kinetic energy of the species arriving to substrate:[a]
$\langle K \rangle_N = 57 \pm 24$ eV (initial $K_N = 94$ eV)
$\langle K \rangle_{Ar} = 4 \pm 2$ eV (initial $K_{Ar} = 21$ eV)
$\langle K \rangle_{Ga} = 3 \pm 2$ eV (initial $K_{Ga} = 22$ eV)

Energy of the species typical of the upper energy part of the distribution[b] arriving to the growing film surface:
$\langle K \rangle_N = 105 \pm 39$ eV (initial $K_N = 153$ eV)
$\langle K \rangle_{Ar} = 9 \pm 7$ eV (initial $K_{Ar} = 40$ eV)
$\langle K \rangle_{Ga} = 15 \pm 10$ eV (initial $K_{Ga} = 60$ eV)

[a]Assuming the initial kinetic energy is the mean value of the species leaving the target.
[b]Calculated by assuming that the initial kinetic energy of the species is mean value plus standard deviation.

can, to a good approximation, be simulated using the parameters of the non-ionized Ar+N$_2$ gas mixture. The deposition pressure and substrate to the target distance of the gas layer were introduced in the Monte-Carlo TRIM[45,46] calculations, where the species and corresponding energies emerging from the target were the input parameters and the energies of the species hitting the growing film surface were the output. The results are shown Table III. The estimated mean energies of Ga and N arriving at the substrate were 3 and 57 eV, but significant amounts of 15 eV Ga and 105 eV N were also expected because of the broad distribution generated by the target collisions.

The main structural aspects of the samples are presented in Figs. 2–4. Fig. 2 shows a section of the grazing angle X-ray diffraction pattern corresponding to the ($10\bar{1}0$), (0002), and ($10\bar{1}1$) planes of the hexagonal lattice of GaN plotted for the different temperatures and substrates. As the figure shows, the films deposited at low temperatures (100 °C) (Fig. 2(a)), present similar GIXRD patterns in the different substrates. The peaks corresponding to (0002) planes are sharper and more intense than those corresponding to ($10\bar{1}1$) are, whereas the ($10\bar{1}0$) plane at ~32° is absent. In films deposited at 600 °C (Fig. 2(b)), the ($10\bar{1}1$) peaks are narrow, and weak) ($10\bar{1}0$) peaks are evident. Greater changes are noticed in Fig. 2(c), corresponding to $T_s = 800$ °C, where the (0002) peak is almost absent and the ($10\bar{1}1$) plane has the highest intensity, particularly on films deposited on silica glass. Furthermore, the difference between the ($10\bar{1}0$) peak and the substrate orientation is remarkable. The peak shows only in the film on a-plane sapphire but is absent in the others. Two small peaks, located at 33.6° and 60.3° only on a-plane sapphire substrate, can be attributed to the substrate because similar peaks are present in the diffractogram of the bare a-plane sapphire substrate (not shown). These small peaks also coincide with the

positions of the Ga$_2$O$_3$ peaks, but because they do not show up in samples on c-plane sapphire and silica glass, the contribution of Ga$_2$O$_3$ is disregarded in the subsequent analysis. The GIXRD 2θ scans in the 30°–40° range of samples deposited at 700 °C and 1000 °C (not shown) are similar to those represented in Fig. 2(c), except that at 1000 °C, the relative intensities of the ($10\bar{1}0$) peaks are bigger than the ($10\bar{1}1$) peaks in all substrates. Also remarkable are the shifts in 2θ in relation to the reported unstressed GaN peaks[50–52] shown in Fig. 2(c).

The differences between the measured 2θ positions of the maxima of ($10\bar{1}0$), (0002), and ($10\bar{1}1$) peaks in the GIXRD measurements and the corresponding positions of the relaxed GaN crystals extracted from a high-quality powder-diffraction pattern as reported by Balkas *et al.*[50] (PDF#50-0792) and Moran e Vickers[51] were plotted in Fig. 3(a). The data correspond to different substrate orientations and temperatures. The estimated errors in $\Delta(2\theta)$ measurements are 0.05°. A clear shift corresponding to a monotonic drop to negative values of δ (2θ) is observed at 700, 800, and 1000 °C in all investigated planes, indicating an increase of the corresponding interplanar distances and stretch of the hexagonal GaN lattice. Using the reported bulk modulus of the GaN, B = 210 GPa,[53,54] the maximum estimated values of the tensile stress occurred in the film deposited at 1000 °C onto a-plane sapphire ($\sigma \sim 9.3$ GPa), corresponding to $\Delta V/V = 0.044$, which is very large and far beyond the expected elastic regime. The absence of cracks in the surfaces of the highly strained films indicates that the observed strains are mainly related to intrinsic stresses. The possible causes of the observed strain and resulting stress are analyzed in Sec. IV. In Figure 3(b), the full widths at half maximum of the GaN for the different diffraction peaks were plotted as a function of the substrate temperature.

(a)

(b)

(c)
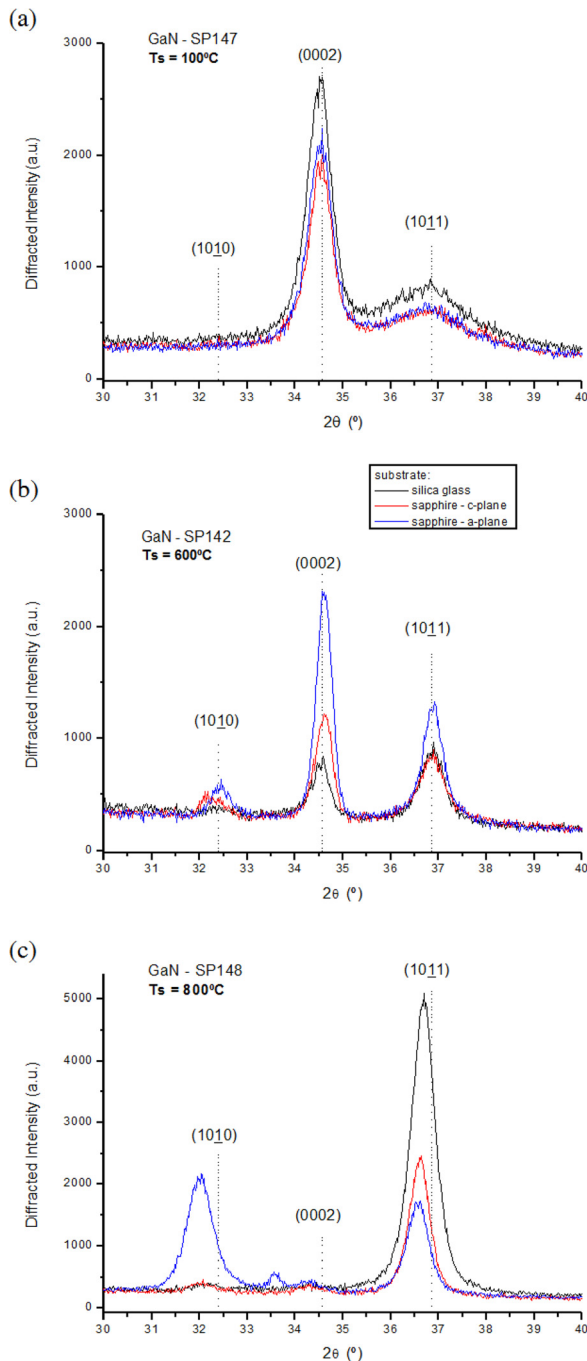
FIG. 2. Grazing incidence X-ray diffraction patterns of GaN films deposited onto different substrates (indicated by lines of different colors). (a)–(c) correspond to samples grown at 100, 600, and 800 °C, respectively. The vertical dotted lines indicate the positions of the peaks in unstrained films reported by Balkas *et al.*[50] (PDF#50-0792).

a)

b)

FIG. 3. (a) Shifts of the measured peak position of different planes relative to high quality diffraction data for unstrained GaN powder (PDF#50-0792).[50] The corresponding diffraction experiments were performed at grazing incidence (1.5°). The analyzed peaks correspond to ($10\bar{1}0$), (0002), and ($10\bar{1}1$) planes, with expected unstressed 2θ positions at 32.388, 34.563, and 36.385, respectively.[50] The different symbols refer to the different diffraction planes, deposition powers, and substrates. The error in 2θ shift of each point is estimated as 0.05°. The blue star placed artificially at room temperature represents the shift in 2θ position of (0002) planes caused by a fluence of $3 \times 10^{13} \, cm^{-2}$, 308 MeV Xe^+ at room temperature, as reported by Zhang *et al.*[63] (b) Full widths at half maximum of the GaN for the different diffraction peaks (indicated in the inset) as a function of the substrate temperature.

Figure 4 shows the rocking curves of the (0002) planes of films deposited at 600 °C onto different substrates. A very broad curve is observed in films deposited on silica glass substrates (Fig. 4(a)). Films on sapphire substrates (*c*- and *a*-planes, respectively, for Figs. 4(b) and 4(c)) produced sharper peaks, with the maxima indicating a texture in which the axis of most [0001] crystallites stay less than 0.5° tilted in relation to the substrate surface normal.

The ω-scan of sample SP142c (600 °C/*c*-plane sapphire) under fixed $2\theta = 34.42°$, Fig. 4(b), displays an intense peak at $\omega = 17.65°$. Although the peak is relatively broad ($\sim$4°) and slightly off the Bragg angle (17.23°) for this set of planes, the result indicates significant orientation texture of the GaN (0002) planes with the *c*-axis of the GaN crystallites in the film placed nearly parallel to the *c*-axis of the sapphire substrate. Indeed, the ω-scan peaks corresponding to the ($10\bar{1}1$) planes were much weaker and broader (position $\omega = 17.6°$, $2\theta = 36.9$, intensity = 850 counts) than the (0002) peaks.

When deposited onto *a*-plane sapphire, the GaN films also displayed a strong orientation texture (Fig. 4(c)). In this situation, the normal to the sapphire substrate (the [$11\bar{2}0$] sapphire axis) was aligned with the [0001] GaN directions, so once again the (0001) GaN planes were nearly parallel to the substrate surfaces, indicating a tendency to epitaxy, which agree with previous reports of GaN epitaxial growth.[1,2,4,10–12,22–26] The reciprocal space map, including

a)

b)

c)

d)
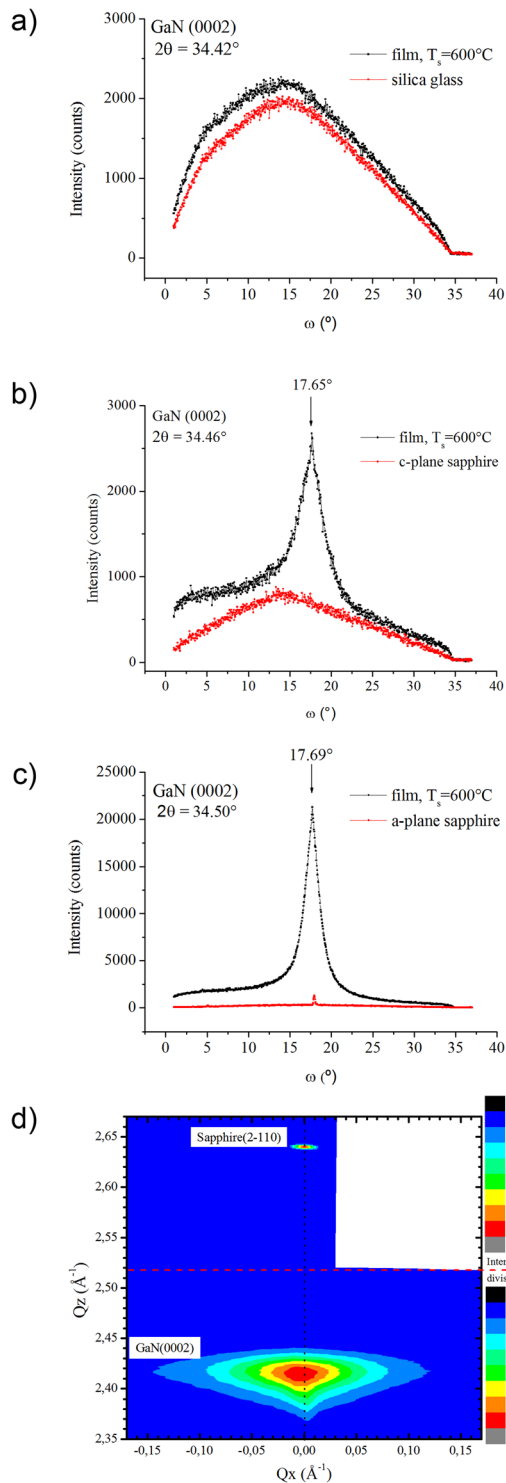
FIG. 4. The ω-scans (a)–(c) and reciprocal space mapping of the (0002) peak of the sample deposited at 600 °C. The ω-scans were made for different substrates: (a) silica glass, (b) *c*-plane sapphire, (c) *a*-plane sapphire, while the reciprocal space mapping (d) was made for the sample deposited onto a-plane sapphire (SP142d).

GaN (0002) and the sapphire ($2\bar{1}10$) reciprocal vector poles, of the sample deposited at 600 °C onto a-plane sapphire [sample SP142d, Figure 4(d)], shows that the angular dispersion of the normal to the (0002) planes is relatively broad. Also the mean value of the x projection of reciprocal vector (Q_x) of the GaN film is slightly shift to negative as compared

to the mean Q_x value of the substrate (0.0035 A^{-1}), so the mean value of the normal to the GaN planes has a slight misalignment to the normal of the ($2\bar{1}10$) planes.

Figures 5(a) to 5(c) display the AFM mapping of the surface of the sample deposited at 800 °C onto different substrates. The surface morphology of the film deposited onto silica glass (Fig. 5(a)) displayed slightly smaller (mean size of 140 nm) and more rounded grain distribution, whereas the films on the sapphire *c*- and *a*-planes displayed grains with more facets and slightly bigger sizes (300 nm), particularly on *a*-plane sapphire. On the latter, a high density of elongated surface structures was also apparent. The surface morphology of samples deposited at 500 °C or below (not shown) was

a)

b)

c)
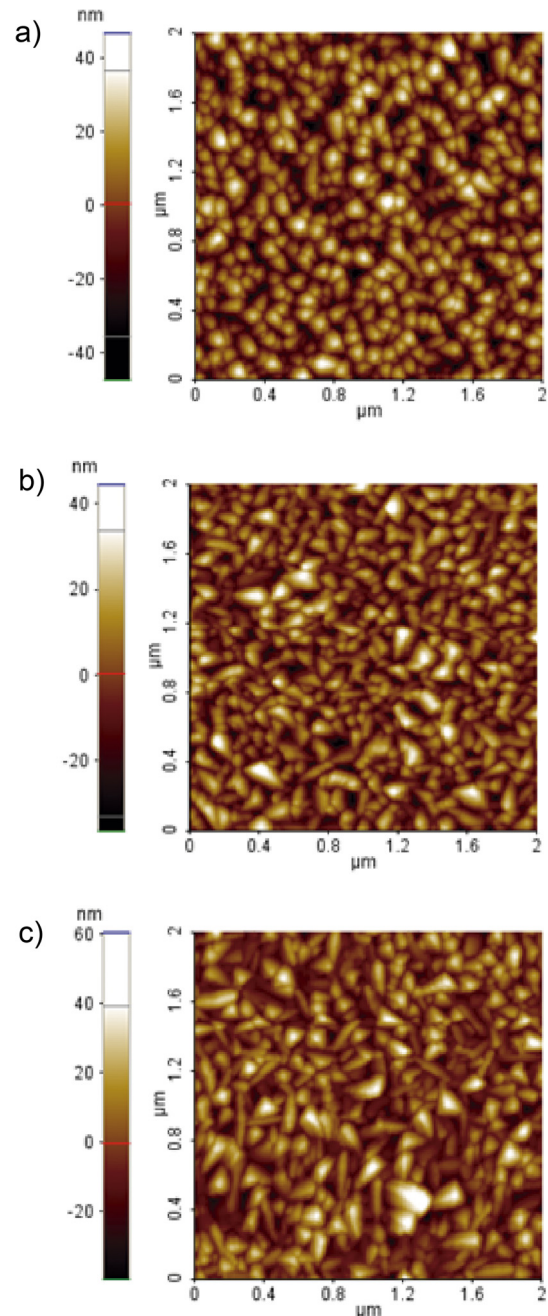
FIG. 5. AFM analysis of the surface of the GaN film deposited by reactive sputtering at 800 °C. Top left: silica substrate. Top right: sapphire c-plane. Bottom: sapphire a-plane.

similar to those displayed in Fig. 5(a), independent of the substrate.

The cross-sectional SEM images of the samples deposited at 300, 600, and 1000 °C onto *a*-plane sapphire substrates are shown in Fig. 6 (middle). Images of the out-of-plane, film-air interface of the samples also shown on the right of Fig. 6(b) and on the left of the others.
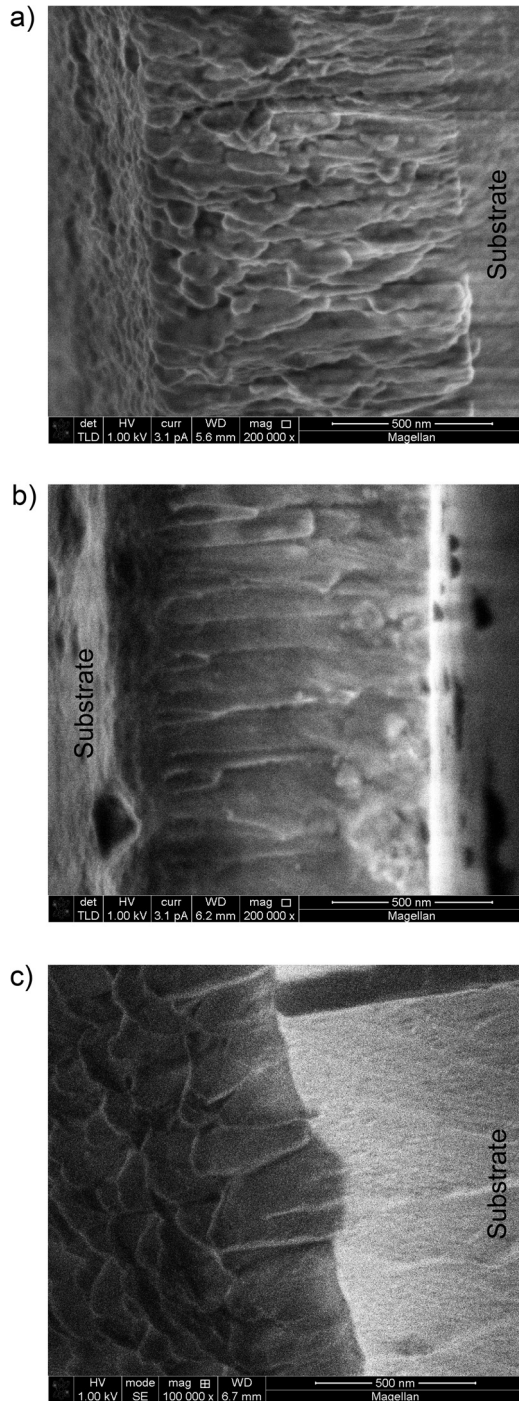
FIG. 6. Secondary electron SEM image of cross sections of GaN films deposited by RF magnetron sputtering (45 W) onto a-plane sapphire at different temperatures. (a) 300 °C, Ts/Tm = 0.21 (SP144d)[49] (b) 600 °C, Ts/Tm = 0.32 (SP142d). (c) and 1000 °C, Ts/Tm = 0.47 (SP150d). The film cross sections are seen in the middle of the pictures. The film air interfaces are displayed in the left region of (a) and (c), and in the right of figure (b) and the cleaved substrate surfaces in the opposite sides. The white line scale bar corresponds to 500 nm.
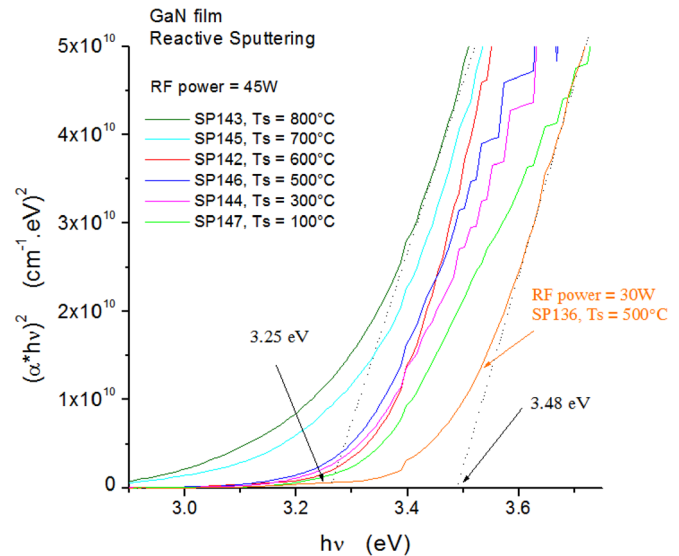
FIG. 7. Absorption edge of GaN films deposited onto silica glass substrates at different temperatures.

The optical absorption edge plots, $(\alpha.h\nu)^2 vs. h\nu$, of the films deposited in different conditions are shown in Fig. 7. A relatively broad range of values of bandgaps (3.25 to 3.48 eV) was found, as indicated by the limiting extrapolation lines. The plotted values correspond to the films deposited onto silica glass substrates. The maximum value of the bandgap corresponds to the samples deposited at $T_s = 500\,°C/45\,W$, and the higher slopes of the absorption edge corresponds to samples deposited at 500 and 600 °C.

IV. DISCUSSION

Important differences that arise in the comparison of GaN produced by reactive sputtering with the traditional epitaxial growth techniques are related to the effect of the impingement of the energetic species on the surface of the growing film. Useful information concerning the energies of the impinging species and the produced damage were provided by the Monte-Carlo TRIM[34,45,46] simulation (Tables II and III) and molecular dynamics results,[35,37,55] respectively.

According to the TRIM results, Ar^+, N_2^+, and N^+ ions at the higher end of the energy distribution (reaching the target with the full V_{bias}) are expected to have energies of the order of 10 eV (Ar^+) and 100 eV (N^+) when they reach the film surface. Most of the sputtered Ga are expected to arrive at the film surface with energies of approximately 3 eV, but a considerable amount coming from the high energy end of the distribution can have energies as high as 25 eV (Table III).

Molecular dynamics simulations by Xiao *et al.*[37] showed that the calculated displacement energies of Ga and N atoms change considerably depending on direction. The displacement energy in the [0001] direction is the highest (78 and 85 eV for N and Ga, respectively), while the corresponding estimated averages are 32.4 eV (N) and 73.2 eV (Ga). In comparing these molecular dynamics simulations with the TRIM results, it is expected that the greater damage in the growing film are produced by the N collisions, while the impinging energy-enhanced Ga atoms are likely to bind

quickly to the film surface (the extra energy would help to overcome the activation energy barrier to bonding) and to promote some compaction of the deposit.

A small decrease (∼4%) in the bias voltage was observed in the $100\,°C \le T_s \le 1000\,°C$ range for the 45 W samples, which slightly changed the energy of the incident ions. In addition, the effects of substrate heating on the thermal distribution of the gases are not significant because of the relatively low pressures. Hence, the present analysis assumes that the energetic distribution of the incident particles was nearly constant, changing only when the RF power changed from 30 W to 45 W.

In the investigation of the structure of the films, the combination of the results of X-ray diffraction using the configurations of grazing incidence, ω-scan, and Bragg-Brentano (in films on silica glass only) showed that the substrate orientation played an important role in the upper range of substrate temperatures (Z_2 zone): it causes important changes in film orientation, revealing some aspects of the well-known tendency of the epitaxial growth of GaN films onto sapphire substrates.[2,6,10,11,14,15,51] Nevertheless, the obtained widths of the rocking curves were much broader than that found in the low-strain materials produced by MOCVD and MBE, which indicate a large density of defects in the analyzed films.

The GIXRD patterns shown in Fig. 2 evidenced that the changes in the texture of the films were a function of the temperature and orientation of the substrate. In association with ω-scans, the results showed that in films deposited at $100\,°C$ (Fig. 2(a)) and $300\,°C$, the texture effects were weak in all tested substrates. At $500\,°C$, 30 W and $600\,°C$, 45 W and higher temperatures, the films deposited onto the sapphire *c*-plane and *a*-plane presented clear effects of orientation texture. The influence of the substrate orientation was also observed on the surface morphology of the samples (Fig. 5). When compared with the film grown onto silica glass (Fig. 5(a)), the faceted features shown in Fig. 5(b) and the elongated features shown in Fig. 5(c) (*a*-plane sapphire substrate) evidence higher anisotropic diffusion in the growth surface. Although observed effects of substrate orientation on film texture were expected for depositions in the $600\,°C–1000\,°C$ range because of the thermal diffusion of precursors,[2,4,9–12] in the present study, the energetic impingement of ions should also play a role.

The 2θ shifts of the more intense diffraction peaks of GaN for different substrates (Fig. 3) display an overall behavior that indicates lattice swelling in films grown at higher substrate temperatures; whereas in depositions at lower temperatures, the effective strains were close to zero. Differently, in epitaxial GaN, compressive stress generally dominates, because of the larger thermal expansion coefficient of sapphire.[51,56–60] Large compressive stresses were also reported in films deposited by RF sputtering for substrate temperatures below $500\,°C$.[25]

Both the previous literature[39–41,51,52,56,61] and our analysis of the data in the present study indicate that the observed lattice swelling (with changes in both a and c parameters of the GaN hexagonal cell) can be attributed to three main factors: (i) the coalescence/merging of the crystallites/interfaces;[56] (ii) the

loss of film material during and after growth; and (iii) impingement of energetic N and the corresponding creation of self-interstitials.[34,41,52,62,63] These points are discussed in more detail in the following.

First is the possibility is that the forces favoring coalescence between grains are responsible for the observed increase in cell volume. The values estimated for the strain and the resulting tensile stress are very large, compared to most reports.[17,25,26,41,62,63] This can be caused by the high adherence of the films to the substrate provided by the energetic deposition, in association with the tendency of the grain interfaces to merge. In SEM images of the cross section of the film deposited at $1000\,°C$ (and *a*-plane sapphire), the grain contours are still apparent (Fig. 6(c)); thus, the merging process is likely to be favored in these conditions.

Second, the loss of film material by the evaporation of Ga and N from the films caused by the relatively high temperature[61] is evidenced by the decrease of the sticking coefficient and consequent decrease in thickness with the increase of temperature (Fig. 1). During the depositions, the imping-ing N atoms from the plasma (having relatively higher energy and partial pressures) tend to refill the vacant sites, whereas the less energetic and lower partial pressure Ga are less likely to reach the vacant sites deeper in the material. After the end of depositions, during the respective temperature decreases, more significant losses of N and Ga are also expected, especially for depositions at higher T_s.

The loss of film material is expected to contribute to the tensile strain, because the film-substrate and grain-grain interfaces tend to keep the original volume of the crystallites, while the loss tend to reduce it. Moreover, considering the intrinsic, microscopic effects, Ga vacancies are expected to produce an increase in the unit cell volume.[52] The tendency to desorb caused by the high temperature, in association with the atomic displacement of Ga atoms from stable locations caused by energetic collisions, are likely to contribute to the swelling of the lattice. In contrast, the N vacancies are expected to produce shrinkage of the unit cell (the Ga atoms in the vacancy tend to be closer than in the regular lattice).[52] In addition, large densities of dislocations and other defects are expected to occur and to favor the diffusion losses.[52,64,65]

Third, if the sputtering deposition and the analysis of ion impingement are considered, tensile microstresses could be generated in the GaN films because of the inclusion of N as an interstitial (the energy of the reflected N is enough to produce this effect). Nevertheless, according to this argument, it is expected that the samples deposited at lower temperatures should also exhibit a pronounced tensile effect, but this was not observed in the present data. The samples at temperatures lower than or equal to $600\,°C$ did not show significant systematic departures of the peaks to the unstressed positions. In addition, the expected tendency of annealing in producing the out diffusion or rearrangement of interstitials and the relaxation of the lattice was not verified, and the opposite effect was observed. Thus, more complex mechanisms should be taken into account.

It is possible that, with efficient channeling, a large number of deep self-interstitials was introduced during growth. This deep interstitial is likely to remain trapped in

the bulk of the material. Thus, because the higher temperatures favored orderly lattices (and annealing of vacancies), the expected strain produced by these self-interstials is larger than expected at low temperatures.

The similarity of the behaviors of the curves shown in Figs. 1 and 3 in the higher range of deposition temperatures ($700\,°C \leq T_s \leq 1000\,°C$) is noteworthy, specifically the correlation between the increase in tensile stress and the decrease in the films' thickness with increasing substrate temperatures. On one hand, the increase on diffusion and desorption with temperature are responsible by the thinning of the film and by shrinking the dimensions of the crystallites and on the other the coalescence among them. The combination of these opposite tendencies is expected to produce a stretching effect on the crystallites. The observed effects largely overcame the compressive stress resulting from the smaller expansion coefficient of GaN in relation to the sapphire substrate, which has been generally observed on epitaxially grown samples.[56,59,60] In the low temperature range ($T_s < 500\,°C$), the thicker layers are expected to decrease the "memory" effect of the film-substrate interface, helped by the wider grain boundaries and amorphous regions present.

It is worth noting that unlike several results reported in the literature,[17,25,26] no cracking or peeling from substrate was observed in SEM, AFM, or the optical confocal microscopies in films at all temperatures, despite the large stress observed in the growth at high temperatures.

As shown in Figs. 5(a) to 5(c), the surface morphology of the sample deposited at $800\,°C$ revealed a marked difference with the substrate kind in correlation with that observed in the GIXRD experiments (Fig. 2(c)). The faceted shape of the films grown on sapphire, especially the elongated structures of the film onto the *a*-plane, evidenced the enhanced surface diffusion of adatoms during growth. If it is interpreted as resulting from the incomplete coalescence of the grains, this morphology also helped to understand the existence of tensile strain in the material. This interpretation is in agreement with the cross sectional SEM images shown in Fig. 6. Grain boundaries showed clearly in the images because of the effects of charging produced by the scanning beam. The set of SEM cross-sectional images are also in qualitative agreement with the Movchan-Demchishin-Thornton[32,33,48] scheme: the sample $T_s = 300\,°C$ in the Z_1 displayed smaller and less defined grains (Fig. 6(a)); the morphology of the sample in the lower Z_2 ($T_s = 600\,°C$) (Fig. 6(b)) had a columnar shape; and in the higher Z_2 ($T_s = 1000\,°C$) (Fig. 6(c)), the grains displayed wider basis. The only unexpected characteristic in the scheme was higher surface roughness of the $T_s = 1000\,°C$ sample. The higher roughness in this scale range is probably associated with the tendency of showing more stable facets in the film-air surface (as the diffusion should be high) and the high tensions present in the grain contours.

The optical band gaps at room temperature in the grown films are lower than expected for the bulk crystal (3.42 eV).[66,67] The only exception is the sample deposited using lower power (30 W), smaller N_2 flow ($N_2/Ar = 1/2$), and $T_s = 500\,°C$. In this case, the determined band gap (3.48 ± 0.05 eV) is very similar to that in the GaN crystal. There is no evidence in the XRD

diffraction of the presence of a cubic phase ($E_g = 3.2$ eV),[2,54] which could in principle be responsible for the observed decrease in band gap. Possible reasons are associated with the increase in lattice parameters.

Rieger *et al.*[59] reported shifts in the photoluminescence caused by substrate-induced biaxial compressive stress: $dE_{PL}/d\sigma = 27 \pm 4$ meV/GPa.[59] If an extrapolation of this value is used as a reference for the variation in the band gap in the tensile range, a decrease as high as 240 meV could be expected in the deposition at $1000\,°C$, corresponding to the estimated tension of ~ 9 GPa. The observed shift of ~ 150 meV (Table I and Fig. 7) was smaller than the mentioned extrapolated value. This difference can be attributed to the fact that the elastic regime should no longer be valid in the high-tension range. Therefore, the important point is that the observed decrease is within the range, so the measured values of the optical gap are compatible with the observed increase in the lattice parameter. Following the same trend, previous density functional theory-based calculations using B3LYP functionals indicated that the increase in d spacing can account for the observed closing of the band gap.[68]

Figure 7 also shows that the slopes of the curves are greater in samples deposited at $500\,°C$ and $600\,°C$. Other samples with absorption edges that were less steep were expected to have higher degrees of structural disorder, in agreement with the structural results: lower stress levels produce a decrease in the defect density of the material. The sample with the best optical characteristics (i.e., highest Eg and edge slope, SP136) was deposited using a lower relative N_2 flow rate ($N_2/Ar = 1/2$) and a lower deposition power (30 W), both of which tended to decrease the energetic collisions of N reflected from the target.

According to the observed results, the desirable effect of the increase in substrate temperature on producing a more ordered GaN film structure was prevented by the stresses that were produced during reactive sputtering, particularly in the planar diode geometry and relatively low deposition pressures that were used. The use of geometries that reduce frontal energetic collisions and/or higher values of the product pressure × target to substrate distance in order to favor the thermalization of the energetic ions coming from the target should produce films that are less defective, but on the other hand lower adherence to the substrate is expected.

Summarizing the main differences between thermal and sputtering processes for the growth of GaN films, it is worth to remark that in processes based only on thermal activation and performed on sub-atmospheric pressures like MOCVD, the temperature of the susceptor plays an important role in activating the precursor species.[13–16] Differently, in reactive sputtering, the substrate temperature has a minor effect on the activation of the impinging species. Because of the relatively low working pressures of reactive sputtering, the activation of precursors is almost exclusively caused by the plasma,[17–27] and thus occurs independently of the substrate temperature. In the growth of GaN by reactive sputtering, the increase in the substrate temperature produces an increase in the vapor pressure of the film, which then produces the sublimation of N and Ga far from equilibrium,

while the incidence of the depositing species is directional and almost exclusively dependent on the parameters of the plasma. Hence, in the present case, the film structure was strongly influenced by the interplay of the plasma energetics and the substrate temperature. The resulting growth mechanism is then rather complex. Consequently, more detailed and systematic studies will be necessary to provide a deeper understanding of the growth process in relation to the corresponding materials' properties.

V. CONCLUSION

GaN films were grown by reactive magnetron sputtering, keeping the distribution of energetic particles constant while varying the orientation and temperature of the substrates. The analysis showed that the wurtzite crystallites of the GaN films displayed a clear orientation texture, favoring the placement of the GaN [0001] axis approximately perpendicular to the sapphire *a*-plane and *c*-plane substrate surfaces, particularly in the substrate temperature range of 500–1000 °C. In addition, in the deposition temperature range of 700–1000 °C, the XRD experiments evidenced a large increase in the interplanar distances, which was compatible with the increase in both *a* and *c* wurtzite lattice parameters of GaN. It can be inferred that the tensile stress produced in the films during the growth were much larger than the extrinsic compressive stress produced by the difference in the thermal expansion coefficients of the film and lattice in the cool-down process after the growth. The films were mechanically stable. No cracks were observed independent of the substrates used, despite the large mean stresses present in samples deposited at 700 °C or higher. It was proposed that the compatibility of the large stresses with mechanical stability was because of the high adherence of the energetic impinging particles to the substrate and to the surface of the growing film, combined with the tendency of the grains to coalesce at deposition temperatures in the 700–1000 °C range. The structural results correlated well with the optical bandgap redshift observed with the increase in substrate temperature.

The best optical and structural results were obtained for films grown using 500 °C, 30 W and 600 °C, 45 W in which the out-diffusion from the film was low, and the benefits of the temperature increase caused by the decrease in defect density were greater than the problems caused by the strongly strained lattice that occurred at higher temperatures.

ACKNOWLEDGMENTS

[1]S. P. DenBaars, D. Feezell, K. Kelchner, S. Pimputkar, C. C. Pan, C. C. Yen, S. Tanaka, Y. J. Zhao, N. Pfaff, R. Farrell, M. Iza, S. Keller, U. Mishra, J. S. Speck, and S. Nakamura, Acta Mater. **61**, 945–951 (2013).
[2]M. A. Reshchikov and H. Morkoc, J. Appl. Phys. **97**, 061301 (2005).
[3]S. Shet, Y. Yan, J. Turner, and M. Al-Jassim, J. Power Sources **232**, 74 (2013).
[4]S. J. Pearton, J. C. Zolper, R. J. Shul, and F. Ren, J. Appl. Phys. **86**, 1 (1999).
[5]C. J. Lewins, D. W. E. Allsopp, P. A. Shields, X. Gao, B. Humphreys, and W. N. Wang, J. Display Technol. **9**, 333 (2013).
[6]F. Scholz, Semicond. Sci. Technol. **27**, 024002 (2012).
[7]C.-C. Chen, C.-H. Chiu, S.-P. Chang, M. H. Shih, and M.-Y. Kuo, Appl. Phys. Lett. **102**, 011134 (2013).
[8]H. C. Hsu, Y. K. Su, S. J. Huang, C. Y. Tseng, C. Y. Cheng, and K. C. Chen, Photon. Technol. Lett., IEEE **23**, 287 (2011).
[9]M. F. Schubert, S. Chhajed, J. K. Kim, E. F. Schubert, D. D. Koleske, M. H. Crawford, S. R. Lee, A. J. Fischer, G. Thaler, and M. A. Banas, Appl. Phys. Lett. **91**, 231114-3 (2007).
[10]T. D. Moustakas, "Growth of III-V nitrides by molecular beam epitaxy," in *Semiconductors and Semimetals*, edited by J. I. Pankove and T. D. Moustakas (Academic Press, San Diego, 1999), Chap. 2, pp. 33–128.
[11]T. Lei, K. F. Ludwig, and T. D. Moustakas, J. Appl. Phys. **74**, 4430 (1993).
[12]C. R. Albernathy, "Growth of group III nitrides from molecular beams," in *GaN and Related Materials*, edited by S. J. Pearton (Gordon and Breach Publishers, Amsterdam, 1997), pp. 53–84.
[13]H. Yoo, K. Chung, S. I. Park, M. Kim, and G.-C. Yi, Appl. Phys. Lett. **102**, 051908 (2013).
[14]X. Ni, Y. Fu, Y. T. Moon, N. Biyikli, and H. Morkoc, J. Cryst. Growth **290**, 166 (2006).
[15]H. Amano, N. Sawaki, I. Akasaki, and Y. Toyoda, Appl. Phys. Lett. **48**, 353 (1986).
[16]E. Richter, C. Hennig, M. Weyers, F. Habel, J. D. Tsay, W. Y. Liu, P. Bruckner, F. Scholz, Y. Makarov, A. Segal, and J. Kaeppeler, J. Cryst. Growth **277**, 6 (2005).
[17]E. C. Knox-Davies, J. M. Shannon, and S. R. P. Silva, J. Appl. Phys. **99**, 073503 (2006).
[18]M. Park, J.-P. Maria, J. J. Cuomo, Y. C. Chang, and J. F. Muth, Appl. Phys. Lett. **81**, 1797 (2002).
[19]J. H. Kim and P. H. Holloway, J. Appl. Phys. **95**, 4787 (2004).
[20]S. Shirakata, R. Sasaki, and T. Kataoka, Appl. Phys. Lett. **85**, 2247 (2004).
[21]B. S. Yadav, S. S. Major, and R. S. Srinivasa, J. Appl. Phys. **102**, 073516 (2007).
[22]T. Miyazaki, T. Fujimaki, S. Adachi, and K. Ohtsuka, J. Appl. Phys. **89**, 8316 (2001).
[23]J. Ross, M. Rubin, and T. K. Gustafson, J. Mater. Res. **8**, 2613 (1993).
[24]Q. X. Guo, A. Okada, H. Kidera, T. Tanaka, M. Nishio, and H. Ogawa, J. Cryst. Growth **237–239**, 1079 (2002).
[25]K. Kusaka, T. Hanabusa, K. Tominaga, and K. Yamaguchi, J. Vac. Sci. Technol. **22**, 1587 (2004).
[26]T. Kikuma, K. Tominaga, K. Furutani, K. Kusaka, T. Hanabusa, and T. Mukai, Vacuum **66**, 233 (2002).
[27]M. Junaid, C. L. Hsiao, J. Palisaitis, J. Jensen, P. O. A. Persson, L. Hultman, and J. Birch, Appl. Phys. Lett. **98**, 141915 (2011).
[28]K. W. Mah, E. McGlynn, J. Castro, J. G. Lunney, J.-P. Mosnier, D. O'Mahony, and M. O. Henry, J. Cryst. Growth **222**, 497 (2001).
[29]J. H. D. da Silva, D. M. G. Leite, A. Tabata, and A. A. Cavalheiro, J. Appl. Phys. **102**, 063526 (2007).
[30]D. M. G. Leite, T. Li, T. Devillers, Z. S. Schiaber, P. N. Lisboa-Filho, J. H. D. da Silva, and A. Bonanni, J. Cryst. Growth **327**, 209 (2011).
[31]M. Junaid, D. Lundin, J. Palisaitis, C.-L. Hsiao, V. Darakchieva, J. Jensen, P. O. A. Persson, P. Sandstrom, W.-J. Lai, L.-C. Chen, K.-H. Chen, U. Helmersson, L. Hultman, and J. Birch, J. Appl. Phys. **110**, 123519 (2011).
[32]J. A. Thornton, J. Vac. Sci. Technol. A **4**, 3059 (1986).
[33]J. A. Thornton and D. W. Hoffman, Thin Solid Films **171**, 5–31 (1989).
[34]H. Gnaser, *Low Energy Ion Irradiation of Solid Surfaces* (Springer-Verlag, Berlin, 1999), p. 293.
[35]E. Despiau-Pujo and P. Chabert, J. Vac. Sci. Technol. A **28**, 1105 (2010); **28**, 1263 (2010).
[36]A. J. Detor, A. M. Hodge, E. Chason, Y. Wang, H. Xu, M. Conyers, A. Nikroo, and A. Hamza, Acta Mater. **57**, 2055–2065 (2009).
[37]H. Y. Xiao, F. Gao, X. T. Zu, and W. J. Weber, J. Appl. Phys. **105**, 123527 (2009).
[38]J. Nord, K. Nordlund, and J. Keinonen, Phys. Rev. B **68**, 184104 (2003).

[39]Yu. V. Trushin, D. V. Kulinov, K. L. Safonov, J. W. Gerlach, Th. Hoche, and B. Rauschenbach, J. Appl. Phys. **103**, 114904 (2008).

[40]S. Sienz, J. W. Gerlach, Th. Hoche, A. Sidorenko, T. G. Mayerhofer, G. Benndorf, and B. Rauschenbach, J. Cryst. Growth **264**, 184 (2004).

[41]R. C. Powell, N. E. Lee, Y. W. Kim, and J. E. Greene, J. Appl. Phys. **73**, 189 (1993).

[42]C. Kim, I. K. Robinson, J. Myoung, K. Shim, M.-C. Yoo, and K. Kim, Appl. Phys. Lett. **69**, 2358 (1996).

[43]J. I. Cisneros, Appl. Opt. **37**, 5262 (1998).

[44]S. H. Wemple and M. Di Domenico, Phys. Rev. B **3**, 1338 (1971).

[45]J. F. Ziegler, J. P. Biersack, and M. D. Ziegler, TRIM-code in the SRIM-2013 package, www.SRIM.org (2013).

[46]J. F. Ziegler, J. P. Biersack, and M. D. Ziegler, *SRIM The Stopping and Range of Ions in Matter* (SRIM Co, Chester MD, USA, 2008), p. 1129.

[47]R. Kinchin and R. S. Pease, Rep. Prog. Phys. **18**, 1 (1955).

[48]B. A. Movchan and A. V. Demchishin, Phys. Met. Metallogr. **28**, 83 (1969).

[49]The melting temperature of GaN ($T_{m,K} = 2700$ K)[10] as well as the corresponding substrate temperatures ($T_{s,K} = 373$ K to $T_{s,K} = 1273$ K) are used in Kelvin, in order to calculate the homologous temperatures T_s/T_m, as required by the M-D-T model (Refs. 32 and 33).

[50]C. Balkas, C. Bascieri, and R. Davis, Powder Diffraction **10**, 266 (1995).

[51]M. A. Moram and M. E. Vickers, Rep. Prog. Phys. **72**, 036502 (2009).

[52]O. Lagerstedt and B. Monemar, Phys. Rev. B **19**, 3064–3070 (1979).

[53]A. Pollian, M. Grimsditch, and I. Grzegory, J. Appl. Phys. **79**, 3343 (1996).

[54]M. E. Levinshtein, S. L. Ruyantsev, and M. S. Schur, *Properties of Advanced Semiconductor Materials* (John Wiley & Sons, New York, 2001), pp. 6–25.

[55]K. Harafuji and K. Kawamura, Jpn. J. Appl. Phys., Part 1 **49**, 011001 (2010).

[56]T. Böttcher, S. Einfeldt, S. Figge, R. Chierchia, and H. Heinke, Appl. Phys. Lett. **78**, 1976 (2001).

[57]M. A. Moram, M. J. Kappers, F. Massabuau, R. A. Oliver, and C. J. Humphreys, J. Appl. Phys. **109**, 073509 (2011).

[58]S. Raghavan, J. Acord, and J. M. Redwing, Appl. Phys. Lett. **86**, 261907 (2005).

[59]W. Rieger, T. Metzger, H. Angerer, R. Dimitrov, and O. Ambacher, Appl. Phys. Lett. **68**, 970 (1996).

[60]T. Kozawa, T. Kachi, H. Kano, H. Nagase, N. Koide, and K. Manabe, J. Appl. Phys. **77**, 4389 (1995).

[61]J. Unland, B. Onderka, A. Davydov, and R. Schmid-Fetzer, J. Cryst. Growth **256**, 33 (2003).

[62]Y. Gao, J. Xue, D. Zhang, Z. Wang, and C. Lan, J. Vac. Sci. Technol. B **27**, 2342 (2009).

[63]L. M. Zhang, C. H. Zhang, L. Q. Zhang, X. J. Jia, T. D. Ma, Y. Song, Y. T. Yang, B. S. Li, and Y. F. Jin, Nucl. Instrum. Methods Phys. Res. B **269**, 1782 (2011).

[64]R. Chierchia, T. Böttcher, H. Heinke, S. Einfeldt, and S. Figge, J. Appl. Phys. **93**, 8918 (2003).

[65]Z. Y. Liu, S. R. Xu, J. C. Zhang, J. S. Xue, X. Y. Xue, M. T. Niu, and Y. Hao, J. Cryst. Growth **343**, 122 (2012).

[66]C. Stampfl and C. G. Van de Walle, Phys. Rev. B **59**, 5521 (1999).

[67]S. Tripathy, R. K. Soni, H. Asahi, K. Iwata, and R. Kuroiwa, J. Appl. Phys. **85**, 8386 (1999).

[68]M. C. Mazini, J. R. Sambrano, A. A. Cavalheiro, D. M. G. Leite, and J. H. D. da Silva, Quimica Nova **33**, 834 (2010).